Magnetic-field-induced formation of exciton magnetic polarons in ZnSe/$Zn_{1-x}Mn_xSe$ quantum-well structures

V. V. Rossin,* F. Henneberger, and J. Puls
Humboldt-Universität zu Berlin, Institut für Physik, Invalidenstrasse 110, Berlin 10115, Germany
(Received 21 September 1995; revised manuscript received 22 December 1995)

cw and time-resolved photoluminescence spectroscopy is used to study ZnSe/$Zn_{1-x}Mn_xSe$ quantum wells with semimagnetic barriers in an external magnetic field. The data demonstrate a change of the dominant energy relaxation mechanism from disorder localization of light-hole excitons at zero-field to heavy-hole exciton interface magnetic polaron formation at intermediate fields and, again, disorder localization of heavy-hole excitons at large magnetic fields. The formation of the interface magnetic polaron is promoted by a magnetic-field-induced type-I–type-II transition for heavy-hole excitons. Despite the transition, neither the exciton lifetime nor its optical oscillator strength is dramatically altered. This is, as we confirm by numerical solution of the two-particle Schrödinger equation, a result of the electron-hole Coulomb interaction. The polaron formation time is initially 110 ps, but decreases with growing magnetic field down to 70 ps ($B=5$ T). A theoretical investigation of the polaron formation dynamics shows that the associated change of the exciton wave function is smaller, the closer the Mn^{2+} spin system is driven into saturation by the external field. As a consequence, the polaron formation time approaches the characteristic Mn^{2+} spin response time. Our measurement uncovers a fast primary localization prior to the polaron process—but also of magnetic origin—that we believe to be necessary to start the polaron formation. [S0163-1829(96)01323-9]

I. INTRODUCTION

In semimagnetic semiconductors, the strong s,p-d exchange interaction between the spins of the extended band states and the localized magnetic ions gives rise to unique magneto-optical properties. The giant Zeeman splitting, Faraday rotation, and optically induced magnetization are well-known examples.[1–4] One of the most interesting phenomena is the formation of a magnetic polaron. Here, the presence of a carrier causes a ferromagnetic alignment of the surrounding magnetic ion spins that, in turn, lowers the energy and leads to autolocalization of the carrier.[5] The fundamental interband excitations of a semiconductor are electron-hole pairs coupled by the Coulomb attraction (excitons). Therefore, even in the situation when only one carrier species interacts significantly with the magnetic ions, the total electron-hole wave function is generally reorganized. The exciton magnetic polaron (EMP) of this kind is the subject of the present paper.

Whether or not a stable EMP can be formed is basically a question of the balance between kinetic and exchange energy.[6] It is thus clear from a simple degree-of-freedom consideration that the dimension of the system plays a crucial role. Indeed, a larger stability range than in three dimensions was recently predicted for quasi-two-dimensional EMP's in quantum wells (QW's).[7,8] Moreover, QW structures of different design (semimagnetic wells and/or barriers) allow the study of assorted spatial configurations of the carrier-ion spin system.[9] A structure of particular interest is a nonmagnetic QW embedded between semimagnetic barriers. Here, the strength of the exchange interaction is determined by the penetration of the exciton wave function into the barrier. In thin QW's, where this penetration is large, a quasi-two-dimensional EMP merely associated with the localization of the carrier in-plane motion occurs.[10] However, the exchange energy can be further increased by a shift of the wave function towards the heterointerface,[11,12] so that its maximum is now close or even inside the barrier. The interface EMP of this kind was first reported for comparatively thick (7-nm) CdTe/$Cd_{1-x}Mn_xTe$ QW's.[13] In order to create a noticeable areal density of Mn^{2+} spins per exciton, localization of the in-plane motion is also required in this case. For realistic QW structures, a theoretical analysis[7] yields, however, that the exchange interaction itself is not sufficient to achieve this. Therefore, a primary localization of different origin, e.g., due to interface roughness, is demanded for both types of EMP's from which their formation subsequently starts. This provided, recent treatments[14,15] have derived a quite simple criterion under what condition the interface EMP exists: the exchange energy available at the interface must be larger than the potential barrier through the band offsets. An examination for the CdTe/$Cd_{1-x}Mn_xTe$ system shows that the band offsets are here too large to meet this criterion.[16] The experimental observation of the interface EMP has remained thus open.

In a previous communication,[17] we have studied ZnSe/$Zn_{1-x}Mn_xSe$ QW structures. This system has a number of features that distinguish it from CdTe/$Cd_{1-x}Mn_xTe$ and favor the formation of an interface EMP. At the same Mn concentration, the band offsets are nearly five times smaller. Through the giant Zeemann effect, the band alignment can be switched from type I to type II by an external magnetic field.[18,19] For superlattice structures with bulky 10-nm wells and relatively small Mn concentration (4–14 %), the observation of a type-II EMP was recently reported.[20] The structures used in our study are vitally different. They consist of true QW's typically of 5-nm width and wide barriers with a Mn content in the range of 20%.

Due to tensile in-plane strain, the light-hole exciton (X_{lh}) is the one of lowest energy, but no EMP is found in this situation. In a magnetic field, the heavy-light hole sequence is reversed and, above a critical field of about 2 T, an interface EMP emerges that is related to the heavy-hole exciton (X_{hh}).

In the present paper, we combine magnetoabsorption, cw and time-resolved photoluminescence (PL) to elucidate the specific nature of the interface EMP in more detail. The unique scenario described above for $ZnSe/Zn_{1-x}Mn_xSe$ QW's allows us to draw a number of conclusions that are not easily accessible by other systems. The heavy- to light-hole crossover gives direct insight into the crucial role played by the band offsets. We are further able to reveal the importance of the electron-hole Coulomb interaction in presence of a type-II band alignment. The magnetic field can be used to adjust the change that the exciton wave function undergoes during the EMP formation. This makes it possible to single out the pure spin response time of the Mn^{2+} ion system and get information about the underlying mechanisms.

II. EXPERIMENT

The $ZnSe/Zn_{1-x}Mn_xSe$ QW structures were grown by molecular-beam epitaxy on (001) GaAs substrates. We have studied structures with a Mn concentration ranging between 16% and 24% and with a QW thickness close to the exciton bulk radius. In the following, we present data for a typical structure consisting of a 0.7-μm-thick $Zn_{0.8}Mn_{0.2}Se$ buffer layer and 5 ZnSe QW's of thickness $d=5$ nm separated by 85-nm-wide $Zn_{0.8}Mn_{0.2}Se$ barriers.

The samples were mounted in the bore of a superconducting split-coil magnet capable of fields up to 12 T and immersed in pumped superfluid helium ($T=1.6$ K). The circularly polarized cw PL and PL excitation (PLE) spectra were studied using a tunable dye laser (Stilbene 3) pumped by an argon-ion laser. The spectra were dispersed by a single 2-m monochromator, with a spectral resolution of 0.3 meV and detected by a photomultiplier. For time-resolved measurements, a synchronously pumped tunable dye laser with a pulse duration of 2 ps and 76-MHz repetition rate was used. In order to avoid sample heating and to keep the excitation density low, the laser spot diameter on the sample was 1 mm and the average optical power 30 mW. After passing a double 0.25-m monochromator in a subtractive dispersion mode, the PL was recorded with a synchroscan streak camera. Time-resolved spectra were constructed using a deconvolution procedure after acquisition of PL traces at a sufficient number of points across the relevant spectral range. Corrections were also made for the jitter of the excitation pulse and intensity fluctuations both measured simultaneously with each trace. The overall spectral and time resolution of the system was 1 meV and 5 ps, respectively.

III. RESULTS

The change of the low-temperature PL and PLE data ($T=1.6$ K) of the QW structure under the influence of an external magnetic field (B) is summarized in Fig. 1. At $B=0$, the light-hole state with angular momentum $J_h=\pm\frac{1}{2}$ is that of lowest energy, because of tensile in-plane strain

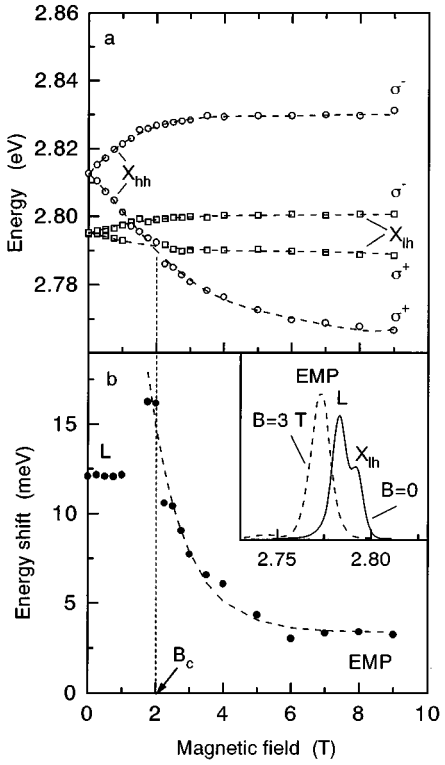

FIG. 1. Energy positions of PLE peaks (a) and energy separation between the lowest PLE and PL peaks (b) versus magnetic field in Faraday geometry. PLE spectra are detected either at L or EMP. Lines are drawn to guide the eye. Inset shows the PL spectra at zero magnetic field and above the X_{lh}-X_{hh} crossover.

across the QW. The energy separation between X_{lh} and X_{hh} is 18 meV. The PL spectrum (inset of Fig. 1, solid line) exhibits a line, due to the recombination of X_{lh} and a second structure labeled L about 10 meV below X_{lh}. The behavior of L resembles that of a donor-bound exciton.[17]

In Faraday geometry (field perpendicular to the QW plane), the exciton spectrum is entirely reorganized. This is demonstrated in Fig. 1(a), which depicts the positions of the exciton resonances as a function of B measured in PLE. A huge Zeeman splitting of the X_{hh} state into σ^+- and σ^--polarized components is seen. The splitting of X_{lh} is markedly less pronounced. Therefore, at a critical field B_c of about 2 T, the σ^+ component of X_{hh} crosses the X_{lh} resonance, so that the lowest excitation in absorption is now that with $J_h=\frac{3}{2}$. In PL, this transition is manifested by the disappearance of the X_{lh} emission and the emergence of a new low-energy line labeled by EMP (inset to Fig. 1, dashed line). At the field strength of its appearance, the energy separation ΔE between the EMP line and the X_{hh} resonance in PLE is 16 meV. As we have studied elsewhere,[17] the variation of ΔE with magnetic field and temperature directly demonstrates that an EMP of X_{hh} is formed. Figure 1(b) shows that ΔE is reduced by a further increase of B and approaches a value close to the disorder induced X_{lh} Stokes shift at $B=0$ of 2.3 meV. The spin of an increasing number of Mn^{2+} ions is now already aligned by the external field and, necessarily, the extra alignment that can be contributed by the photoexcited exciton decreases (saturation regime). Though the EMP line appears in almost the same spectral

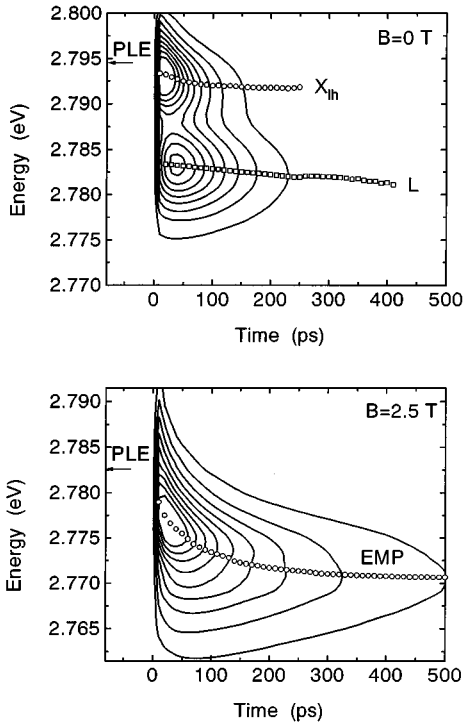

FIG. 2. Contour plots of the PL at $B=0$ and 2.5 T, respectively. Open symbols given the position of the PL peaks. The arrows mark the position of the lowest PLE peak.

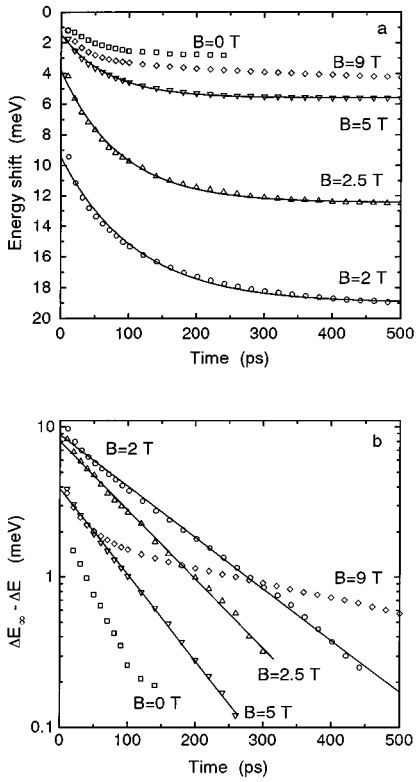

FIG. 3. Time evolution of the PL peaks for different magnetic fields (a—linear scale, b—semilogarithmic). Lines are exponential fits. The position of the PLE peak at the respective B is defined as the zero of the energy scale in (a).

range as L and both lines can be hardly separated near B_c, they are definitively of different origin, as demonstrated by the time-resolved PL data presented below. There is thus no EMP contribution in the X_{lh} emission at $B<B_c$ that can be separated from the disorder-induced Stokes shift. The reason why X_{hh} and X_{lh} behave so strikingly different with respect to the EMP formation will be stressed in Sec. IV.

The above scenario of EMP formation is entirely confirmed by time-resolved PL data. Figure 2 displays contour maps of the QW PL in a time-energy plane at various magnetic fields. In addition, the time evolution of the PL maxima is depicted. In these measurements, the excitation was resonant to excited QW exciton states. However, no substantial change of the PL dynamics was observed for excitation energies above the barrier band gap.

The most notable result at zero magnetic field is the coexistence of L and X_{lh} during their quite similar lifetimes. The X_{lh} peak has a faster rise time (10 ps) and dominates in the PL spectrum at early times (<50 ps), while later L becomes the dominant structure. Both lines undergo a small (≈ 2 meV) low-energy shift in time. Most of the X_{lh} Stokes shift seen under cw excitation is developed within the first 50 ps. As already mentioned above, these findings exclude an interpretation of L as an EMP of X_{lh} at zero magnetic field.

At magnetic fields above B_c, the scenario revealed by the time-resolved data is profoundly altered. Only a single line is present in the PL spectrum. But that line undergoes now a distinctly larger low-energy shift than X_{lh} and L at $B=0$. This transient shift of the X_{hh} emission energy uncovered by the time-resolved data visualizes directly the process of the EMP formation and the related raise of the alignment of the Mn^{2+} spins. Figure 3 displays the time evolution of the PL peaks at different magnetic fields. The peak position is given relative to the lowest PLE maximum, which defines $\Delta E=0$ at the respective magnetic field in Fig. 3(a). For $B=0$, only the temporal dependence of X_{lh} is shown. In consistency with the cw results, the transient PL shift becomes less when the magnetic field is further increased and the EMP formation suppressed. At $B\geqslant 9$ T, when the Mn^{2+} spins are fully saturated, the time evolution is no longer of magnetic origin, but reflects the localization of X_{hh} in the disordered QW potential similarly as for X_{lh} at $B=0$.

A significant portion ΔE_0 of the total PL shift ΔE_∞ is already established within a time shorter than the 5-ps resolution of our set up. On the other hand, a single-exponential time dependence

$$\Delta E(t)=\Delta E_0+\Delta E_t[1-\exp(-t/\tau_f)] \qquad (1)$$

provides a very satisfactory fit to the data on the time scale experimentally accessible. Here, $\Delta E_t=\Delta E_\infty-\Delta E_0$ is the part of the shift resolved in time and τ_f its characteristic time constant. A semilogarithmic plot of $[\Delta E_\infty-\Delta E(t)]$ in Fig. 3(b) displays indeed a very good linearity, except for the data at 9 T exhibiting a slow down of the transient PL shift at longer times. Figure 4 summarizes the values obtained for ΔE_0, ΔE_t, and τ_f, as a function of B. Suppression of not only the time resolved, but also the fast primary PL shift with increasing magnetic field is clearly seen. In addition, the time constant turns out to be markedly enhanced at medium

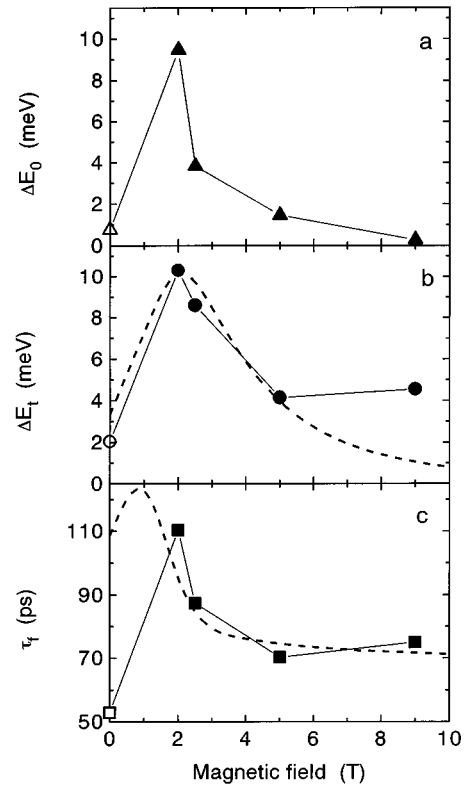

FIG. 4. Primary (a) and time-resolved (b) PL shifts, as well as the time constant (c) versus magnetic field. At $B \geq B_c$ (true EMP regime) data are shown by full symbols, while at $B < B_c$—by open symbols. Solid lines are to guide the eye. The dashed curves represent calculated data for an EMP (see Sec. V).

magnetic fields. We emphasize that neglecting ΔE_0 would yield completely misleading results.

Figure 5 presents decay curves of the spectrally integrated PL at characteristic magnetic fields. The decay time taken at the $1/e$ point increases first by a factor of 1.8 until the X_{lh}-X_{hh} crossover, but exhibits only a slight decrease when B is further enlarged and does not recover to its zero-field value in the saturation regime.

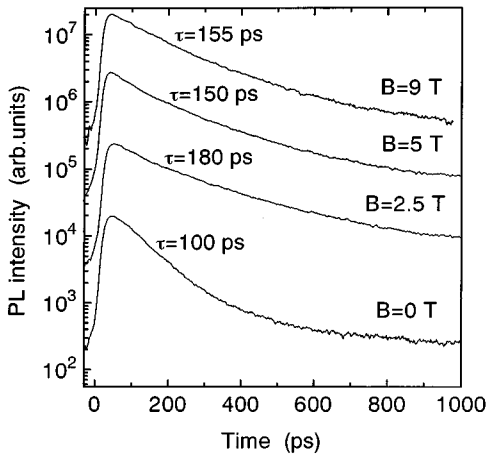

FIG. 5. Spectrally integrated PL decay kinetics for various magnetic fields. The curves are arbitrarily shifted along the vertical axis. The values of τ are decay times taken at the $1/e$ point.

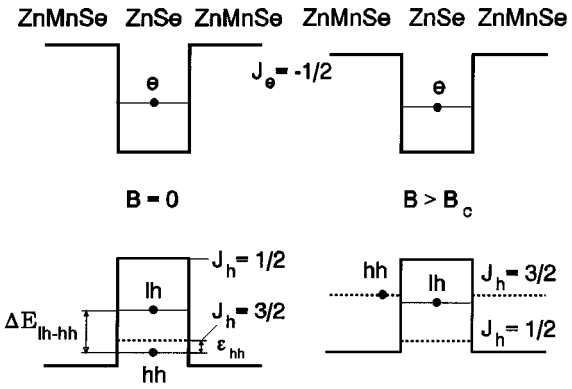

FIG. 6. Band-gap alignment in a $ZnSe/Zn_{0.8}Mn_{0.2}Se$ QW at $B=0$ (left) and $B>B_c$ (right). The heavy-hole band edge is marked by dashed lines.

IV. MAGNETIC FIELD-INDUCED TYPE-I–TYPE-II TRANSITION

The EMP formation is dominated by the exchange interaction of the holes, since the electron coupling is a factor of five smaller in $Zn_{1-x}Mn_xSe$.[21] The qualitatively different behavior of X_{hh} and X_{lh} is caused by the quite different strain-induced valence-band offsets. The total-energy-gap discontinuity ($\Delta V_e + \Delta V_h$) at the present Mn concentration is 100 meV for the light and 65 meV for the heavy hole, respectively.[22] For the present QW thickness, the large offset prevents formation of either type of EMP's for X_{lh}. For X_{hh}, however, it becomes clear, from the band scheme depicted in Fig. 6, that a type-I–type-II transition takes place. Namely, the field-induced X_{lh}-X_{hh} crossover requires a type-II alignment for the heavy hole if its confinement energy $\varepsilon_{\mathrm{hh}}$ at $B=0$ is less than the splitting $\Delta E_{\mathrm{hh\text{-}lh}}$ between the exciton states of 18 meV.[23] A standard potential-well calculation based on a heavy-hole mass of $m_{\mathrm{hh}}=0.49m_0$ (Ref. 24) yields an upper limit of $\varepsilon_{\mathrm{hh}}=14$ meV, assuming that 100% of the total offset lies in the valence band. We conclude thus that the criterion for an interface EMP of X_{hh} is surely met in the present QW structure. Though the type transition occurs at lower fields, formation of an EMP starts only above B_c when X_{hh} is the exciton ground state. Below B_c, there is not enough time because of the very rapid heavy- to light-hole conversion (<1 ps).[25]

The type-I–type-II transition is commonly believed to decrease drastically the exciton oscillator strength and increase its radiative lifetime as a result of the spatial separation of electrons and holes confined now in different layers.[19,26] Our study does not indicate any dramatic change of the electron-hole separation under the type-I–type-II transition. The increase of the PL decay time (Fig. 5) from below to above B_c is only very moderate. Two possibilities have to be considered. First, if the exciton decay is governed by the radiative recombination, the data directly demonstrate that the electron-hole overlap is indeed weakly altered. Second, in the case of a dominant nonradiative recombination, the actual increase of the radiative lifetime might be much larger. However, this would imply a drop of the PL yield, whereas we observe even a raise.[17] To confirm that the exciton oscillator strength is not drastically changed, an independent

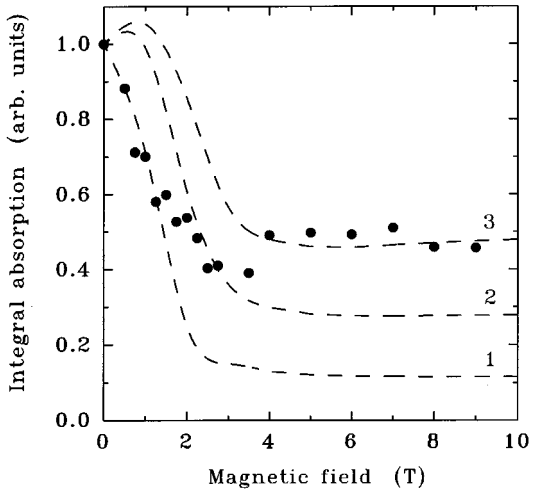

FIG. 7. Spectrally integrated σ^+-$X_{\rm hh}$ absorption (symbols) versus magnetic field. Dashed lines—variational calculation of the $X_{\rm hh}$ oscillator strength for different relative valence-band offsets $V_{\rm hh}/(V_e+V_{\rm hh})$: 1–23 %; 2–26 %; 3–31 %.

magnetoabsorption measurement on a structure with substrate and buffer layer removed was performed. In consistency with the PL data, the spectrally integrated absorption of the lowest σ^+-$X_{\rm hh}$ component exhibits a decrease by a factor of only 2.2 at $B\approx B_c$ and no remarkable further reduction at larger fields (Fig. 7).

It is the electron-hole Coulomb attraction that assures the wave-function overlap required to see clear absorption resonances even when the heavy-hole band alignment is of type II. In order to illustrate this quantitatively, we have solved the Schrödinger equation for $X_{\rm hh}$,

$$\left[\sum_{i=e,h}\left\{-\frac{\hbar^2}{2m_i}\frac{\partial^2}{\partial z_i^2}+V_i(z_i,B)\right\}-\frac{\hbar^2}{2\mu}\frac{1}{\rho}\frac{\partial}{\partial\rho}\rho\frac{\partial}{\partial\rho}-\frac{e^2}{\varepsilon|\mathbf{r}_e-\mathbf{r}_h|}\right]\Psi(\mathbf{r}_e,\mathbf{r}_h)=E\Psi(\mathbf{r}_e,\mathbf{r}_h), \tag{2}$$

in a variational approach using a trial wave function,[27]

$$\Psi(\mathbf{r}_e,\mathbf{r}_h)=C\phi_e(z_e)\phi_h(z_h)\exp\{-[\rho^2+(z_e-z_h)^2]^{1/2}/a\}, \tag{3}$$

where ρ is the in-plane electron-hole relative coordinate, z_e (z_h) the electron (hole) position in growth direction, and C a normalization constant. The reduced in-plane mass μ of $X_{\rm hh}$ is given in terms of the electron, heavy-hole and light-hole masses along the z axis by $1/\mu=1/m_e+1/4m_{\rm hh}+3/4m_{\rm lh}$. The functions ϕ_e and ϕ_h are calculated self-consistently by numerical solution of the single-particle Schrödinger equations for a given value of the variational parameter a changed as long as the energy is minimized. The external magnetic field enters the calculation via the effective band offsets,

$$V_i(z_i,B)=\theta(|z_i|-d/2)\{\Delta V_i-V_{mi}B_{5/2}[g\mu_B B/k_B(T+T_0)]\} \qquad (i=e,h). \tag{4}$$

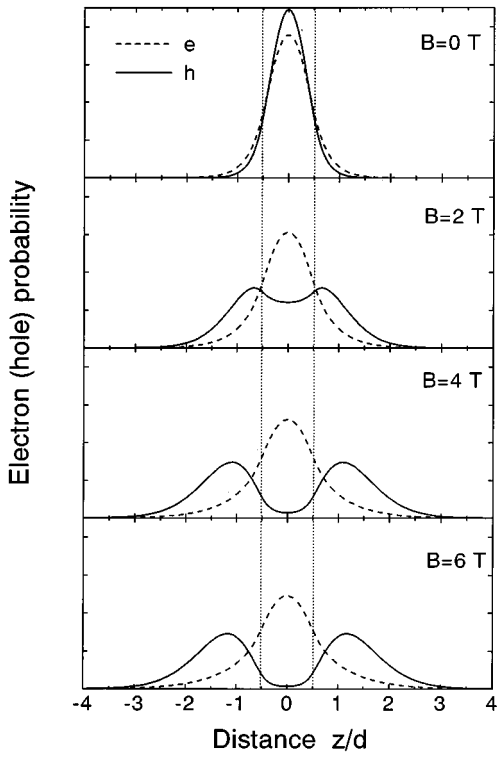

FIG. 8. Calculated probability distribution of the electron (dashed lines) and hole (solid lines) along the quantization axis (z) at different values of the magnetic field. Dotted lines mark the well-barrier interfaces. The variational parameter a (in units of bulk Bohr radius) for increasing fields is 0.90, 1.05, 1.22, and 1.24, respectively.

Here, $\theta(z)$ is the Heaviside function, d the well thickness, and ΔV_i are the zero-field potential barriers. The magnetization of the Mn^{2+} ions is treated in mean-field approximation yielding the Brillouin function $B_{5/2}$, with the Mn^{2+} g factor. The prefactor is given by $V_{mi}=1/2xS_0\alpha_i$, with the Mn concentration x and the exchange constants α_i. The phenomenologically introduced quantities T_0 and S_0 account for antiferromagnetic pairing of the Mn^{2+} spins.[21] Figure 8 depicts the calculated electron and hole probability distributions along the z direction of the $X_{\rm hh}$ ground state for various magnetic fields. The parameter set used is $m_e=0.160m_0$ (Ref. 28), $m_{\rm hh}=0.49m_0$ (Ref. 23), $m_{\rm lh}=0.145m_0$ (Ref. 28), $\varepsilon=8.8$ (Ref. 28), $\alpha_e=0.26$ eV (Ref. 21), $\alpha_h=1.31$ eV (Ref. 21), $S_0=0.58$, and $T_0=4.4$ K. The latter two parameters were adjusted to get the Zeeman shift of $X_{\rm hh}$ observed experimentally. Though no precise value of the relative band discontinuity is known for $ZnSe/Zn_{1-x}Mn_xSe$, it is sure that most of the total offset stems from the conduction band. In Fig. 8, $\Delta V_e=45$ meV and $\Delta V_{\rm hh}=20$ meV is assumed. Due to the lighter mass, however, the penetration of the electron into the barrier is larger than for the hole at $B=0$. This behavior reverses with increasing magnetic field, as a result of the stronger exchange coupling of the valence band. Figure 8 directly demonstrates the associated type transition, but the significant electron-hole overlap maintained through the Coulomb interaction, even at high magnetic fields, is also evident. We note that this result is crucially related to the magnitudes of both the conduction-band offset and well

width. Only when these quantities are small enough, the Coulomb attraction can cause the electron wave function to follow that of the hole and to penetrate indeed deeper into the barrier. The optical oscillator strength is related to the exciton wave function by

$$f_x \sim \left| C \int_{-\infty}^{\infty} \phi_e(z)\phi_h(z)dz \right|^2 . \tag{5}$$

The result of the calculation for different relative heavy-hole valence-band offsets is presented in Fig. 7. The agreement between experiment and theory is reasonably well. Both the magnitude of the oscillator strength decrease and its saturation at high magnetic fields is reproduced. Near $B=0$, since the electron wave function extends initially deeper into the barrier, the growing penetration of the holes causes first a weak increase of the oscillator strength in the calculation. This slight effect may be masked by a number of reasons in real QW structures, as, for instance, fluctuations of the Mn concentration.

V. EMP FORMATION DYNAMICS

The dynamics of the EMP formation is controlled by two processes. First, it needs time to align the spins of the Mn^{2+} ions. That means relaxation in the Zeeman-split Mn^{2+} spin sextuplet and dominant population of the $-\frac{5}{2}$ ground state. We assume that this process can be characterized by a single time constant τ_s. Note, that both spin and energy relaxation are involved in τ_s. Second, the exciton wave function changes during the EMP formation and by this the strength of the carrier-ion exchange coupling. Therefore, the EMP formation time may be markedly larger than τ_s.[29,30]

The primary, unresolved PL shift in our experiments is too fast (<5 ps) to be correlated with relaxation in the Mn^{2+} spin system. We, thus, identify the characteristic time constant τ_f of the resolvable shift at $B>B_c$ with the EMP formation time. The 100-ps range found here is in good accord with similar studies for quasi-two-dimensional EMP's in CdTe/$Cd_{1-x}Mn_x$Te (Ref. 31) and $Cd_{1-x}Mn_x$Se/ZnTe (Ref. 32) QW's. This is reasonable since the spin relaxation of the localized Mn^{2+} ions should not differ very much in these heterostructures. Following a recent consideration[30] of the EMP formation problem, we rule out spin-lattice relaxation of isolated ions and spin diffusion as mechanisms involved in the present case. The former takes place on a much longer time scale[33] and the latter would provide a nonexponential time behavior. A possible mechanism compatible with the experimentally observed time range is nonscalar spin-spin scattering[30,34] that does not conserve the total spin of the ion system. In addition, we believe that the energy dissipation is most likely accomplished by Mn^{2+} clusters that possess a strongly enhanced spin-lattice relaxation rate[33]—in particular, triads are very efficient.[35] Before discussing the influence of an external field upon the EMP dynamics, we note that the exciton lifetime is always larger than τ_f. This guarantees that an EMP close to the stable state is developed under the present conditions.

As clearly seen from Fig. 4, an increase of the magnetic field causes a decrease of the EMP formation time. The data so far reported in the literature on this aspect are rather conflicting. Time-resolved PL studies[36] on $Cd_{1-x}Mn_x$Te and $Cd_{1-x}Mn_x$Se have yielded a distinct quadratic increase of τ_f with B. Contrary, a field-induced decrease of τ_f was observed in dynamical magnetization measurements[37] on the same material group and explained by a field-induced enhancement of the spin-lattice relaxation rate. This was indeed observed for the relaxation of isolated ions, but spin-spin interaction contributing essentially to the EMP formation in our study was found to be field independent.[33] On the other hand, the change of the exciton wave function—in the present case of an interface EMP, the shift towards the semimagnetic layer—is less when a sufficient number of Mn^{2+} spins is already prealigned by the external field. As a consequence, τ_f will approach the pure spin response time τ_s. Consistently, as seen from Fig. 4, the decrease of τ_f is accompanied by a respective decrease of the EMP energy. This conclusion is entirely confirmed by a theoretical analysis of the interface EMP dynamics presented next.

Our approach is based on an adiabatic approximation.[30,38] The presumption behind this approximation is that the wave function follows instantaneously the magnetization, while it takes the finite time τ_s for the magnetization to react on a change of the wave function. In that case, the term

$$V_{ex,i} = \theta(|z_i - d/2)V_{mi} \int_0^t \frac{dt'}{\tau_s} \exp\left(-\frac{t-t'}{\tau_s} \right) \times \left\{ B_{5/2}\left[\frac{g\mu_B[B + B_{\rm eff}(\mathbf{r}_i, t')]}{k_B(T+T_0)} \right] - B_{5/2}\left[\frac{g\mu_B B}{k_B T_0} \right] \right\} , \tag{6}$$

$$B_{\rm eff}(\mathbf{r},t) = \frac{\alpha_h}{2g\mu_B} \Omega_0 \int \Psi^2(\mathbf{r}_e, \mathbf{r}, t)\mathbf{d}^3\mathbf{r}_e \tag{7}$$

(Ω_0: volume of the primitive cell) has to be added to V_i in the Schrödinger equation (2). Here, the time t enters as an external parameter on which now also the exciton wave function $\Psi(r_e, r_h, t)$, the effective exchange field $B_{\rm eff}(r,t)$, and the EMP energy $E(t)$ depend on. In $B_{\rm eff}$, only the hole contribution has to be accounted for (see above).

We look for a solution of the form

$$\Psi(\mathbf{r}_e, \mathbf{r}_h, t) = \Psi_e(\mathbf{r}_e, t) \cdot \Psi_h(\mathbf{r}_h, t), \tag{8}$$

$$\Psi_i(\mathbf{r}_i, t) = \phi_i(z_i, t) \frac{\eta_i(t)}{\sqrt{\pi}} \exp\left[-\frac{1}{2}\eta_i^2(t)\rho_i^2 \right], \tag{9}$$

where both electron and hole, as well as in- and out-plane motion are separated.[39] At first glance, this seems to be in conflict with the discussion of the magnetoabsorption data in the previous section. However, the situation in PL is quite different. The primary, unresolved shift ΔE_0 demonstrates that the exciton has already undergone a localization of different origin before the EMP formation starts. Besides simplicity, this justifies a less accurate treatment of the Coulomb interaction and the use of Gaussians for the in-plane motion. Unlike a previous treatment[12] of the steady-state interface EMP, the wave functions in z direction are not assumed in Gaussian form. Since the electron exchange is neglected, ϕ_e (z_e) is time independent and simply the analytically known wave function of the well potential $V_e(z_e, B)$. Using

these well deliberated simplifications, we are left with the following equation for the hole wave function:[40]

$$-\frac{\hbar^2}{2m_{\rm hh}}\frac{\partial^2\phi_h}{\partial z_h^2}+\left(\Theta(|z_h|-d/2)\left\{V_h(z_h)-V_{mh}\int_0^t\frac{dt'}{\tau_s}\exp\left(-\frac{t-t'}{\tau_s}\right)\int_0^1 dq\left[B_{5/2}\left(\frac{g\mu_B B+\frac{1}{2}\alpha_h\Omega_0\eta_h^2\phi_h^2(z_h,t')q}{k_B(T+T_0)}\right)\right.\right.\right.$$

$$\left.\left.\left.-B_{5/2}\left(\frac{g\mu_B B}{k_B(T+T_0)}\right)\right]\right\}-\frac{e^2}{\varepsilon}\eta\sqrt{\pi}\int_{-\infty}^{+\infty}dz_e\phi_e^2(z_e)\exp[\eta^2(z_e-z_h)^2][1-\mathrm{erf}(\eta|z_e-z_h|)]\right)\phi_h(z_h,t)$$

$$=\left(E_h(t)-\frac{\hbar^2\eta_h^2}{2m_{h\|}}-\frac{\hbar^2\eta_e^2}{2m_e}\right)\phi_h(z_h,t), \quad (10)$$

with $\mathrm{erf}(x)$ as the error function. Here, the inverse in-plane radii η_e and η_h enter via $\eta=\eta_e\eta_h/(\eta_e^2+\eta_h^2)^{1/2}$. Assuming that η_h is fixed by the primary localization process,[11,12] we reduce finally the number of variational parameters to one. The EMP formation is then characterized by two processes: (i) shift of the hole (already localized in plane) towards the semimagnetic barrier and (ii) in-plane localization of the electron through Coulomb interaction.

The solution procedure is as follows. We start at $t=0$ when no EMP effect is present due to the inertia of the spin system. Then, we calculate numerically $\phi_h(z_h,0)$ for different $\eta_e(0)$ until the energy of the localized exciton is minimal. At a time $t>0$, the exchange term in (10) is enumerated using all functions $\phi_h(z_h,t')$ obtained at previous times $t'<t$. Then, we determine $\phi_h(z_h,t)$ and $\eta_e(t)$ by the same procedure as at $t=0$. The calculations are repeated until a stationary solution is reached. The total EMP energy E and polaronic shift ΔE can be expressed by

$$E(t)=\varepsilon_e+E_h(t), \quad (11)$$

$$\Delta E(t)=E(0)-E(t), \quad (12)$$

where ε_e is the electron energy in the potential $V_e(z_e,B)$. Note, that electron-hole interaction is contained in $E_h(t)$. Besides the parameters given in Sec. IV, we used $\Omega_0=4.55\times10^{-23}$ cm^3 and $1/\eta_h=14$ Å adjusted so that $E(0)-E(\infty)$ is equal to the experimental value of the time-resolved shift ΔE_t at $B=2$ T (10 meV).

Figure 9 displays the calculated transient $X_{\rm hh}$ EMP shift at different magnetic fields. In agreement with the above expectations, the EMP formation needs a markedly longer time than τ_s and depends nonmonotonous on B. The transients can be fairly well fitted by single exponentials shown by dashed curves in Fig. 9. The values for τ_f obtained from this fit ($\tau_s=70$ ps independent of B) and the respective total EMP shifts $\Delta E(\infty)$ are plotted as a function of B in Fig. 4, together with the experimental data. For a heavy-hole valence-band offset of 25 meV used in the computations, the critical field of the type-I–type-II transition is $B_c=1.34$ T. Both τ_f and $\Delta E(\infty)$ exhibit maxima near B_c. The maximum of τ_f is at $B<B_c$ and related to the largest change of the hole wave function. Its evolution in time at $B=2$ T is displayed in Fig. 10. Conversely, $\Delta E(\infty)$ is maximal at $B>B_c$, where an optimum between the exchange energy increase caused by the hole wave function change and saturation of Mn^{2+} ions by the external field is achieved.

Let us now discuss the fast, unresolved PL shift ΔE_0 observed prior to the EMP formation. It points at an additional mechanism involved in this process, which has not been discussed so far in the literature. Since the magnitude of ΔE_0 is strongly correlated with the external field (see Fig. 4), this mechanism must be of magnetic origin as well. It has been recently found that photoexcitation of carriers can create magnetic imprints in the Mn^{2+} system that live much longer than the carriers themselves.[41] A memory effect of that kind could generate a background magnetization in our 76-MHz repetition experiments. In order to clarify this, we have reduced the pulse separation from 13.1 to 1.7 ns by a double-pulse technique. No effect on ΔE_0 was found, nor did we observe any change of ΔE_0 with the excitation density. This proves that indeed a process faster than 5 ps is involved. We attribute the initial PL shift to a primary localization of excitons by magnetic fluctuations. Statistically, there are regions where the spins of two or more neighbored Mn^{2+} ions are ferromagnetically arranged. In contrast to the EMP, the carrier but not the Mn^{2+} spins must be now aligned in order to localize excitons in these regions. This

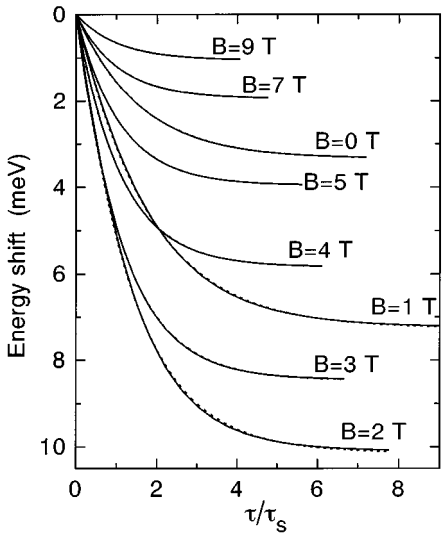

FIG. 9. Calculated transient $X_{\rm hh}$ EMP shift at different magnetic fields. Dashed curves represent single-exponential fits.

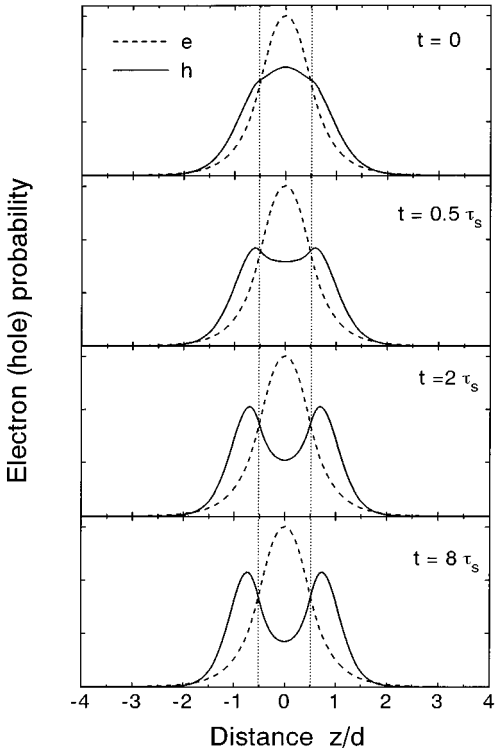

FIG. 10. Calculated probability distribution of the electron (dashed lines) and hole (solid lines) along the quantization axis (z) at different times during the process of EMP formation. Dotted lines mark the well-barrier interfaces.

defines a much shorter time domain as carrier-spin scattering runs on a 1-ps scale or even faster.[42]

The time-resolved PL data demonstrate further the fundamental change of exciton energy relaxation induced by the magnetic field: It turns first from disorder localization (X_{lh}) at $B=0$ to EMP formation at $B>B_c$ and again back to disorder localization (X_{hh}) in the saturation regime. The process of disorder localization is not characterized by a single time constant, since it slows down when the exciton gets deeper into the band tail.[43] This behavior is most clearly observed at $B=9$ T [Fig. 3(b)], proving again that the exciton dynamics is here completely different from the true EMP regime. The same is true for $B=0$, but both the smaller exciton lifetime and Stokes shift make the slowing-down effect less visible.

VI. SUMMARY

We have demonstrated the existence of an interface EMP in $ZnSe/Zn_{1-x}Mn_xSe$ QW structures. Magnetoabsorption data evidence conclusively (i) a type-I–type-II transition for heavy holes and, at somewhat higher magnetic fields, (ii) a heavy-light hole crossover. It turns out both experimentally and theoretically that account of the electron-hole Coulomb interaction is mandatory for an adequate description of the exciton oscillator strength and lifetime under type-II band alignment. While (i) shows that the criterion for the existence of a heavy-hole interface EMP is fulfilled, (ii) is required to switch off the otherwise very rapid heavy- to light-hole conversion. The large light-hole offset blocks the formation of an EMP associated with this valence band. PL data gained under short pulse excitation directly resolve in time the EMP formation and the related polarization of the Mn^{2+} ion system. The transient shift of the EMP line is in a good approximation single exponential with a characteristic time constant of initially 110 ps. As a result of the less pronounced change of the hole wave function close to the saturation regime, the formation time decreases with increasing magnetic field and approaches the pure spin response time of the Mn^{2+} ion system. A theoretical analysis of the EMP formation dynamics based on an adiabatic approximation reproduces the experimental findings reasonably well. A significant portion of the total PL shift is established during a time shorter than the 5-ps experimental resolution. This fast primary localization is also of magnetic origin and can be attributed to the capture by magnetic fluctuations of the Mn^{2+} system. It will be interesting to study other configurations of the carrier-ion system using $ZnSe/Zn_{1-x}Mn_xSe$ QW structures.

ACKNOWLEDGMENTS

The authors thank N. Hoffman and J. Griesche for the sample growth, D. R. Yakovlev, A. V. Kavokin, K. V. Kavokin, and W. Heimbrodt for helpful discussions. One of us (V.V.R.) is grateful to the Alexander von Humboldt Foundation for financial support.

*Permanent address: A. F. Ioffe Physico-Technical Institute, St. Petersburg 194021, Russia.

[1] J. K. Furdyna, J. Appl. Phys. **65**, R29 (1988).
[2] O. Goede and W. Heimbrodt, Phys. Status Solidi B **146**, 11 (1988).
[3] D. D. Awschalom, J. Warnock, and S. von Molnar, Phys. Rev. Lett. **58**, 812 (1987).
[4] H. Krenn, K. Kaltenegger, T. Dietl, J. Spałek, and G. Bauer, Phys. Rev. B **39**, 10 918 (1989).
[5] P. A. Wolff, in *Diluted Magnetic Semiconductors*, edited by J. K. Furdyna and J. Kossut, Semiconductors and Semimetals Vol. 25 (Academic, London, 1988), p. 413.
[6] T. Kasuya, A. Yanase, and T. Takeda, Solid State Commun. **8**, 1543 (1970); M. A. Krivoglaz, Usp. Fiz. Nauk **111**, 617 (1973) [Sov. Phys. Usp. **16**, 856 (1974)].
[7] C. Benoit à la Guillaume, Phys. Status Solidi B **175**, 369 (1993).
[8] A. V. Kavokin and K. V. Kavokin, Semicond. Sci. Technol. **8**, 191 (1993).
[9] G. Mackh, W. Ossau, D. R. Yakovlev, A. Waag, T. Litz, and G. Landwehr, Solid State Commun. **88**, 221 (1993).
[10] D. R. Yakovlev, W. Ossau, G. Landwehr, R. N. Bicknell-Tassius, A. Waag, S. Schmeusser, and I. N. Uraltsev, Solid State Commun. **82**, 29 (1992).
[11] C. E. T. Gonscalves da Silva, Phys. Rev. B **32**, 6962 (1985).
[12] J.-W. Wu, A. V. Nurmikko, and J. J. Quinn, Phys. Rev. B **34**, 1080 (1986).
[13] A. V. Nurmikko, X.-C. Zhang, S.-K. Chang, L. A. Kolodziejski, R. L. Gunshor, and S. Datta, Surf. Sci. **170**, 665 (1986).
[14] C. Benoit à la Guillaume, M. Combescot, and Yu. G. Semenov, in *Proceedings of the 22nd International Conference on the Phys-*

ics of Semiconductors, Vancouver, Canada, 1994, edited by David J. Lockwood (World Scientific, Singapore, 1994), p. 2481.

[15] A. V. Kavokin, Phys. Rev. B **51**, 7613 (1995).

[16] D. R. Yakovlev, G. Mackh, W. Ossau, W. Waag, G. Landwehr, R. Hellmann, and E. O. Göbel, in *Proceedings of the 22nd International Conference on the Physics of Semiconductors, Vancouver, Canada, 1994* (Ref. 14), p. 2613.

[17] V. V. Rossin, J. Puls, and F. Henneberger, Phys. Rev. B **51**, 11 209 (1995).

[18] A. Petrou, W. C. Chou, X. Liu, J. Warnock, and B. T. Jonker, J. Lumin. **52**, 175 (1992).

[19] E. Deleporte, T. Lebihen, B. Ohnesorge, P. Roussignol, C. Delalande, S. Guha, and H. Munekata, Phys. Rev. B **50**, 4514 (1994).

[20] C. G. Poweleit, L. M. Smith, and B. T. Jonker, Phys. Rev. B **50**, 18 662 (1994).

[21] A. Twardowski, M. von Ortenberg, M. Demianiuk, and R. Panthenet, Solid State Commun. **51**, 849 (1984).

[22] U. Streller, N. Hoffmann, A. Schülzgen, J. Griesche, H. Babucke, F. Henneberger, and K. Jakobs, Semicond. Sci. Technol. **9**, 1 (1994).

[23] In this discussion, we have neglected a slight difference in the X_{hh} and X_{lh} binding energies.

[24] B. Sermage and G. Fishman, Phys. Rev. B **23**, 5107 (1981).

[25] A. Schülzgen, F. Kreller, F. Henneberger, M. Lowisch, and J. Puls, J. Cryst. Growth **138**, 575 (1994).

[26] J. E. Golub, K. Kash, J. P. Harbison, and L. T. Florez, Phys. Rev. B **41**, 8564 (1990).

[27] J. Warnock, B. T. Jonker, A. Petrou, W. C. Chou, and X. Liu, Phys. Rev. B **48**, 17 321 (1993).

[28] *Intrinsic Properties of Group IV Elements and III-V, II-VI, and I-VII Compounds*, edited by O. Madelung and M. Schulz, Landolt-Börnstein, New Series, Group III, Vol. 22, Pt. a (Springer, Berlin, 1987).

[29] D. R. Yakovlev, W. Ossau, A. Waag, R. N. Bicknell-Tassius, G. Landwehr, K. V. Kavokin, A. V. Kavokin, I. N. Uraltsev, and A. Pohlmann, in *Proceedings of the 20th International Conference on the Physics of Semiconductors, Beijing, China, 1992*, edited by P. Jiang and H.-Z. Zheng (World Scientific, Singapore, 1992), p. 1136.

[30] T. Dietl, P. Peyla, W. Grieshaber, and Y. Merle d'Aubigné, Phys. Rev. Lett. **74**, 474 (1995).

[31] D. R. Yakovlev, W. Ossau, G. Landwehr, R. N. Bicknell-Tassius, A. Waag, S. Schmeusser, I. N. Uraltsev, A. Pohlmann, and E. O. Göbel, J. Cryst. Growth **117**, 854 (1992).

[32] D. D. Awschalom, M. R. Freeman, N. Samarth, H. Luo, and J. K. Furdyna, Phys. Rev. Lett. **66**, 1212 (1991).

[33] T. Strutz, A. M. Witowski, and P. Wyder, Phys. Rev. Lett. **68**, 3912 (1992).

[34] T. Moriya, Phys. Rev. **120**, 91 (1960).

[35] D. Scalbert, Mater. Sci. Forum. **182-184**, 451 (1995).

[36] J. J. Zayhowski, R. N. Kershaw, D. Ridgley, K. Dwight, A. Wold, R. R. Galazka, and W. Giriat, Phys. Rev. B **35**, 6950 (1987).

[37] D. D. Awschalom, J. M. Halbout, S. von Molnar, T. Siegrist, and F. Holtzberg, Phys. Rev. Lett. **55**, 1128 (1985).

[38] K. V. Kavokin, Fiz. Tverd. Tela **35**, 1624 (1993) [Phys. Solid State **35**, 818 (1993)].

[39] In this case, the operator $1/\mu\partial^2/\partial\rho^2$ in Schrödinger equation (2) must be replaced by $1/m_e\partial^2/\partial\rho_e^2+1/m_{h\|}\partial^2/\partial\rho_h^2$, where $m_{h\|}$ is the in-plane hole mass.

[40] A similar approach was used by A. Mauger, N. S. Almeida, and D. L. Mills, Phys. Rev. B **38**, 1296 (1988), in single-carrier magnetic polaron steady-state calculations for semimagnetic superlattices without taking into account exciton effects.

[41] J. J. Baumberg, S. A. Crooker, D. D. Awschalom, N. Samarth, H. Luo, and J. K. Furdyna, Phys. Rev. B **50**, 7689 (1994).

[42] M. R. Freeman, D. D. Awschalom, J. M. Hong, and L. L. Chang, Phys. Rev. Lett. **64**, 2430 (1990).

[43] E. Runge, A. Schülzgen, F. Henneberger, and R. Zimmermann, Phys. Status Solidi B **188**, 547 (1995).